Publishing House
AKAPIT

COMPUTER METHODS IN MATERIALS SCIENCE
Informatyka w Technologii Materiałów

Vol. 9, 2009, No. 1

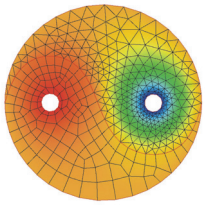

THERMO-MECHANICAL FORMING OF Al-Mg-Si SHEET

A.H. (TON) VAN DEN BOOGAARD[1], SRIHARI KURUKURI[2], MANOJIT GHOSH[2], ALEXIS G. MIROUX[2]

[1]*University of Twente, Enschede, The Netherlands*
[2]*Materials Innovation Institute, Delft, The Netherlands*
Corresponding Author: a.h.vandenboogaard@utwente.nl (A.H. van den Boogaard)

Abstract

In warm forming of aluminum sheet, the temperature and strain rates vary considerably. In simulations, the material model must be capable to predict stresses within this wide range. Here, the physically based Nes model is used to describe the behavior of AA6061-T4 sheet material under warm forming conditions. A significant change of earing behavior is found between room temperature and 250 ºC. Crystal plasticity calculations showed a reasonable correspondence of changing r-values if extra slip systems are considered at high temperatures. Satisfactory results are obtained for simulation of tensile tests and cylindrical deep drawing.

Key words: warm forming, aluminum, material model, deep drawing, Nes model

1. INTRODUCTION

In recent years aluminum alloys are increasingly used in the automotive industry in order to reduce weight. However, aluminum alloys usually show lower room temperature formability, compared to mild steel. One way to overcome the poor formability of aluminum sheet is by temperature enhanced forming. In this process, parts of the tools are heated and other parts are cooled, in order to increase the formability. Forming of 5xxx series at elevated temperatures has been reported by many researchers [1-5]. Recently researchers are inclined to 6xxx series alloys with the intention to achieve improved formability at warm temperatures. The Al-Mg-Si alloys have good corrosion resistance, and obtain high strength, controlled by the precipitates formed during the aging treatment. Therefore, the age hardening response of these alloys is very significant and hence control of precipitation during thermo-mechanical treatment is critical for attaining optimal alloy performance. This process is industrially more challenging and more complex in terms of microstructure-mechanical behavior relationship.

Experience with temperature controlled forming processes is lacking and numerical models are beneficial in optimizing the forming processes. The applicability of commonly applied constitutive models for aluminum is limited in terms of varying strain, strain rate, temperature and changing microstructure. Particularly in warm forming the strain rate and temperature influence cannot be ignored. Material models based on consideration of the underlying physical processes are expected to have a larger range of usability in this respect.

In cylindrical deep drawing, earing is a prominent indicator of anisotropy of sheet material. Appearance of ears is directly related to undesirable effects like thickness variations. The formation of ears at room temperature has been widely investigated and the relation with the crystallographic texture has been established. The earing behavior at elevated temperature is much less documented. In the present paper the relation between plastic anisot-

ISSN 1641-8581

ropy and crystallographic texture as a function of deformation temperature is investigated. Deep drawing experiments with AA6061 alloy are compared with numerical predictions.

2. EXPERIMENTS

Aluminum alloy AA6061 has been used for the present investigation. The material was cold rolled, solutionized and naturally aged (T4). The sheet thickness is 1.2 mm. The alloy contains 0.95 Mg, 0.62 Si, 0.2 Cu and 0.35 Fe in wt%.

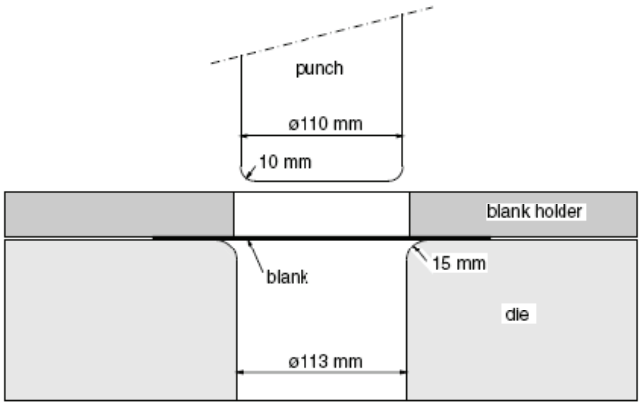

Fig. 1. *Dimensions of the tools for cylindrical cup deep drawing.*

The sheet has been deep-drawn at room temperature and at 250 ºC using a 1000 kN hydraulic press. Experiments were performed with a tool set of which the dimensions are given in figure 1. All experiments were performed with blanks of 220 mm. Blanks were drawn up to a depth of 64 mm with punch velocity 83 mm/min and blank holder pressure of 4.1 MPa at room temperature and with punch velocity 74 mm/min and blank holder pressure 2.5 MPa at 250 ºC. For warm deep drawing, the die and the blank holder were heated by heat rods while the punch was water cooled and kept below 30 ºC. The blank was heated up in contact with the die and was hold for 30 s at 250 ºC before being drawn. Drawing was stopped before the blank completely flowed inside the die. The cup was water quenched after warm drawing. The foot-print of the cups was measured as a parameter of plastic anisotropy. The distance between the cup central axis and the outer circumference was measured and plotted as a function of the angle to the rolling direction.

Tensile tests were performed at room temperature and 250 ºC with the thermo-mechanical simulator Gleeble 3800. Tensile specimens were taken at several angles to the rolling direction and deformed to 10% at a strain rate of 0.01 s^{-1} to measure r-values. The texture of the as-received material has been measured by X-ray diffraction while those of the deformed specimens have been measured by EBSD. The {200}, {220}, {111}, and {311} pole figures were measured and orientation distribution functions (ODFs) were calculated by the series expansion method, with the assumption of orthorhombic sample symmetry.

Figure 2(a) shows that increasing the deformation temperature from room temperature to 250 °C affects the normal anisotropy for all directions but does not change the r-value profile much. At both temperatures the r-value shows a minimum at 40–50° to the rolling direction. Deformation temperature also strongly influences the earing profile of the drawn cups (figure 2(b)). At room temperature a 4-fold symmetry is observed with ears along RD and TD, while at 250 °C the earing profile exhibits a 2-fold symmetry although it shows a tendency to maintain a small local maximum along the rolling direction (0° and 180°).

a)

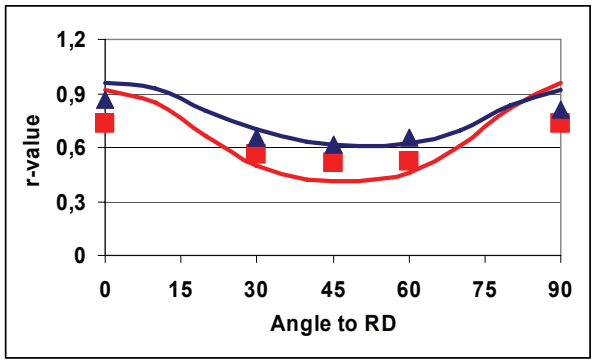

b)

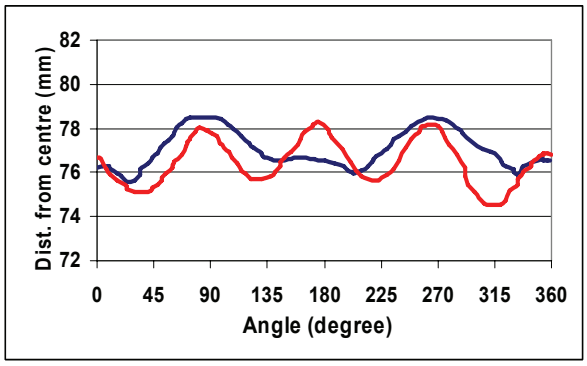

Fig. 2. *a) r-value measured by tensile tests (symbols) and calculated by VPSC model (lines). b) Drawn cup foot-print representing the earing profile at room temperature and 250 ºC.*

The orientation distribution function (ODF) of the AA6061-T4 sheet shows a texture dominated by Cube grains and an η-fibre ($\varphi_1 = \varphi_2 = 0^\circ$) with a weaker Goss component as shown in figure 3. Figure 4 shows the texture in the flange along the rolling direction after deep drawing at room temperature (RT) and at 250 ºC. It can be well noticed

that the texture changes after deformation while the textures obtained after drawing at both temperatures are qualitatively similar. For both textures the maximum has been found close to P with an orientation spread along the α-fibre ($\phi = 45^{\circ}, \varphi_2 = 0^{\circ}$) and towards Cube. There is also an η-fibre between Goss and Cube. Hence it can be observed that temperature did not bring much change in the deep-drawing texture.

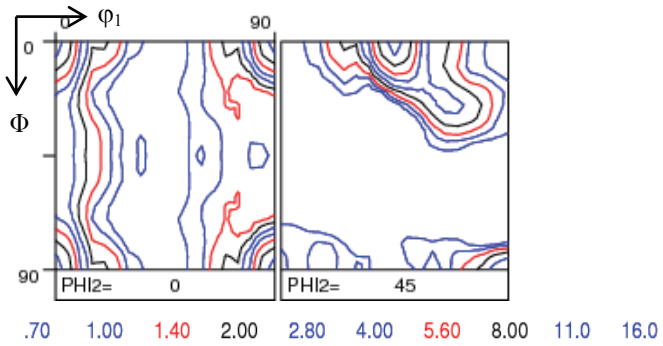

Fig. 3. ODF for AA 6061-T4 sheet calculated from XRD measurement.

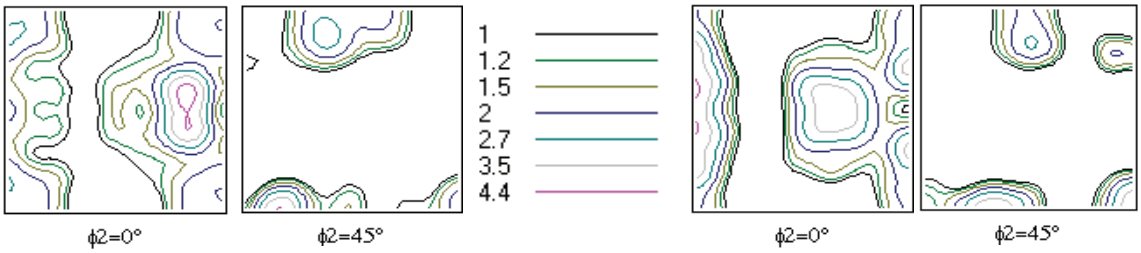

Fig. 4. ODF in the flange after drawing (a) at RT and (b) at 250 ºC.

A visco-plastic self consistent model [6] was used to further investigate the effect of temperature on plastic deformation by assuming that temperature controls the critical resolved shear stresses (CRSS), that means the number of activated slip systems. At room temperature only the octahedral slip systems {111}<110> are allowed, while at 250 ºC four families of slip systems {111}<110>, {110}<110>, {100}<110> and {112}<110> are possible with respective CRSS ratio 0.9:1:1.1:1. The initial experimental texture is discretized with 2000 orientations. The modeled r-value curves with 1 and 4 slip systems respectively are shown in figure 2(a). The results at room temperature compare qualitatively well with the experimental measurements. The CRSS ratio of the four families of slip systems mentioned above have been obtained by fitting the calculated r-values to the r-values measured at 250 ºC. It is evident that by introducing more slip systems it is possible to increase the overall r-value and to obtain an r-value profile close to the experimental one. It can be concluded that, although textures are similar at different temperatures, the activation of different families of slip systems directly affects the r-value profile.

3. MATERIAL MODEL

In this work, the standard model for plastic deformation is used: a combination of a yield function to transform a 3-dimensional stress state to a scalar equivalent stress and a hardening model to determine the size of the elastic domain by isotropic hardening. In the present study, the anisotropic yield function of Vegter [7] is used. For temperature and strain-rate sensitive work hardening, a physically based work hardening model by Nes [8] is used, in which the evolution of microstructure is defined by three internal state variables. The model developed by Nes and coworkers, has earlier been referred to as ALFLOW and MMP (Microstructure based Metal Plasticity) model but will here simply be referred to as the Nes model. The model approach relies on a multi parameter description for the microstructure evolution by combining models for the dislocation storage problem with models for dynamic recovery of network dislocations and sub-boundary structures. The model also includes the thermal stress contributions, static contributions from clusters and constituents along with the contributions from precipitates. Hence the model would give an adequate description for stress-strain behavior at various strain rates and temperatures along with strain rate jumps. The unified nature of the model is characterized in its general applicability, covering both low and high temperature properties of metals, in the form of a fully integrated work hardening description. Extensive presentations of the work hardening part of the model are given in [8,9,10].

3.1. Microstructure evolution

At small strains, the stored dislocations are arranged in a cell structure characterized by a cell size,

δ, cell walls of thickness h and dislocation density ρ_b and a lower dislocation density within cells ρ_i. At large strains the cell walls have collapsed into sub-boundaries of a well defined misorientation φ as shown in figure 5. In the Nes model only ρ_i, δ and φ are independent state variables. The microstructure evolution is obtained by solving a set of differential equations describing the evolution of these parameters. Leaving out the details these can in principle be written as:

$$\frac{d\rho_i}{d\gamma}=\frac{d\rho_i^+}{d\gamma}+\frac{d\rho_i^-}{d\gamma};$$

$$\frac{d\delta}{d\gamma}=\frac{d\delta^-}{d\gamma}+\frac{d\delta^+}{d\gamma}; \qquad (1)$$

$$\frac{d\varphi}{d\gamma}=\frac{d\varphi^+}{d\gamma}+\frac{d\varphi^-}{d\gamma}$$

Here, γ is the resolved shear strain, which is defined as the algebraic sum of resolved shears of each slip system in the Taylor theory and interpreted as an average of the grains in this context. $d\rho_i^+/d\gamma$ and $d\delta^-/d\gamma$ are storage terms, describing different ways of athermal storage of dislocations, whereas $d\rho_i^-/d\gamma$ describes dynamic recovery of cell interior dislocations by dipole annihilation. $d\delta^+/d\gamma$ represents subgrain growth at elevated temperatures. Modeling of the misorientation, $d\varphi/d\gamma$, is currently based on a phenomenological approach. Explicit expressions for these terms can be found in [8,10].

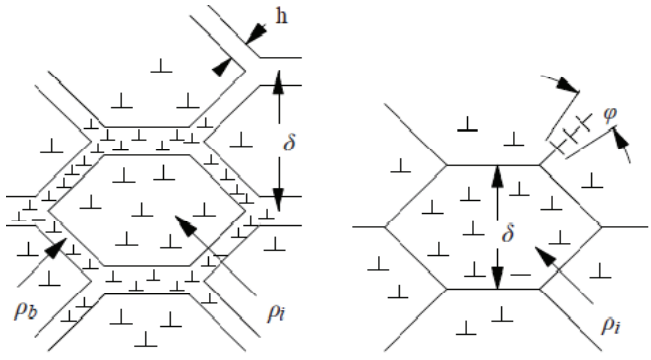

(a) Small deformations (b) Large deformations

Fig. 5. *Schematic presentation of the dislocation cell structure.*

3.2. The flow stress

The flow stress, τ, at a constant microstructure is commonly defined in terms of a thermal stress component, τ_t, and an athermal component, τ_a, so that $\tau=\tau_t+\tau_a$. The thermal component (also referred to as the effective stress) is due to short range interactions between mobile dislocations and intersecting stored ones, dragging of jogs, and elements in solid solution. The athermal component characterizes the rate- and temperature-independent interaction of dislocations with long range barriers. In the treatments by Nes and co-workers [8-10], the stress required for dislocation migration is written as

$$\tau=\tau_t+\tau_p+\tau_{cl}+\alpha_1 Gb\left[\Gamma_1\left(\frac{q_c}{\delta\sqrt{\rho_i}}\right)\sqrt{\rho_i}+\Gamma_2\left(\frac{q_c}{\delta\sqrt{\rho_i}}\right)\frac{q_c}{\delta}\right]+\hat{\alpha}_2 Gb\left[\Gamma_2(0)\frac{1}{\delta}+\frac{1}{D}\right] \qquad (2)$$

The Orowan stress τ_p is due to non-deformable particles. The clustering stress, τ_{cl}, due to clusters formed by supersaturated alloying components with low diffusivity (Fe, Mn, Si). The α_1-term represents the contribution from stored dislocations and the $\hat{\alpha}_2$-term represents the contribution from subgrains and grain boundaries. G is the shear modulus, b is the Burger's vector, δ and D are the cell/sub-grain size and grain size respectively. The functions Γ_1 and Γ_2 are statistical distribution functions of sub-grain sizes within each grain.

In applications of the model the stress tensor at a macroscopic continuum scale is required representing contributions from many grains of various crystallographic orientation and microstructure. In forming operations the texture changes are small and the anisotropy can be captured by the Vegter yield locus, providing a computational cost efficient approach.

In figure 6, the simulated stress-strain curves are plotted for the Nes model, together with the experimental data. The stress-strain curves for temperatures of 25 ºC, 150ºC and 250 ºC are plotted in figure 6(a) for a strain rate of $\dot{\varepsilon}=0.01\text{s}^{-1}$ and in figure 6(b) for a strain rate of $\dot{\varepsilon}=0.1\text{s}^{-1}$. At higher strain rate and at temperatures below 150ºC the model performs quite well. For the higher temperatures, i.e., at 250 ºC the differences are slightly larger. It can also be observed that at low strain rate and temperatures below 150 ºC the initial yield stress is underestimated with the Nes model.

In the experiment at 250ºC the lower strain rate yields a slightly higher stress than the higher strain

rate, which looks unusual. A possible explanation could be that at lower strain rate more time is available for dynamic precipitation. However, as can be seen in figure 6 the Nes model cannot describe the effect of dynamic precipitation.

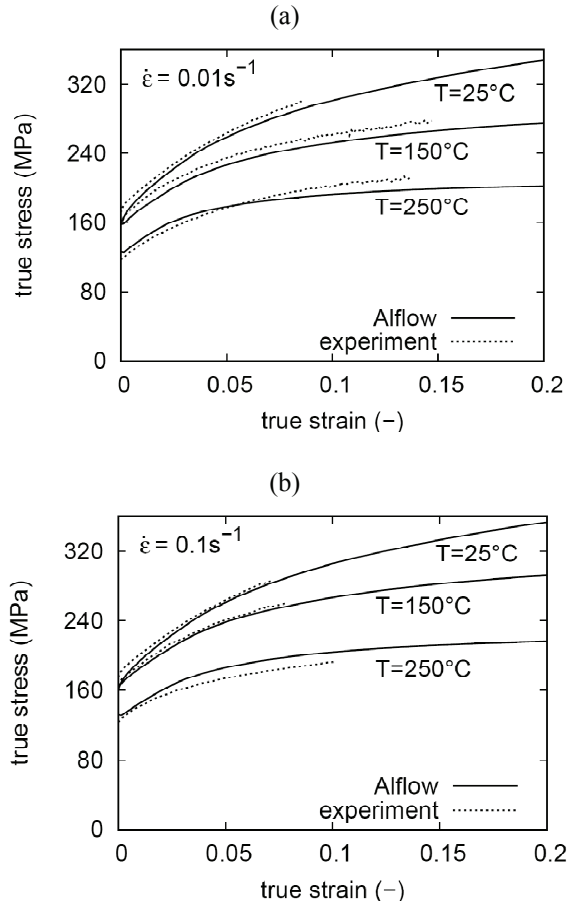

Fig. 6. *True stress-strain curves – experiments and model.*

4. SIMULATION OF CYLINDRICAL CUP DEEP DRAWING

The industrial relevance of the implemented material model is discussed in terms of a case study concerned with warm deep drawing of cylindrical cups. Orthotropic symmetry was assumed for the material model. A quarter of the blank was modeled and boundary conditions were applied on the displacement degrees of freedom to represent the symmetry. The sheets were modeled with 998 discrete Kirchhoff triangular shell elements with 3 translational, 3 rotational and 1 temperature degree of freedom per node. The tools were modeled as rigid contours with a prescribed temperature. Simulations with the Vegter yield locus and the Nes hardening model implemented in the in-house implicit code DiekA are performed at various temperatures. The global convergence criterion was set to 0.5% relative unbalance force.

4.1. Friction

The friction between tool and work piece is one of the least known factors in the simulations. Friction tests on an AA5754-O material, steel tools and a similar lubricant as used here at room temperature showed a friction coefficient of 0.06, which is lower than the value of 0.12 that is commonly used based on simulation experience. Experiments at high temperatures showed values varying between 0.12 and 0.18, both for a temperature of 175 ºC and 250 ºC. In the deep drawing process, the contact and friction conditions can be different than in the friction test, due to a locally different geometry and normal pressure.

To investigate the influence of the friction on the force–displacement curve and the thickness prediction, a parameter study was performed for a flange temperature of 175 ºC. In figure 7 the influence of friction on the punch force is shown for an analysis with the 1-parameter Bergström model [5]. In three analyses, the friction coefficient below 90 ºC, μ_l, was kept at 0.06, but the friction coefficient above 110 ºC, μ_h, was subsequently set to 0.06, 0.12 and 0.18. A linear interpolation was used between these temperatures. With a friction coefficient of 0.18 the calculated punch force–displacement diagram resembles the experimental one quite well. As a result of the increased friction, however, the predicted thickness strain deteriorates (see figure 7).

As an alternative parameter set, the friction coefficient for all tool blank contact was set at 0.12. This is compared with the original set with a friction coefficient of 0.12 between die and blank and blank holder and blank and a friction coefficient of 0.06 between punch and blank. Interestingly, increasing the punch–blank friction has almost no effect on the punch force–displacement curve. The predicted thickness of the bottom area, however, improves considerably, while the predicted thickness in wall and flange hardly changes. This shows that the friction conditions are significant parameters in the simulation and the current uncertainties should be resolved. For the simulations in the next section the experimentally determined friction coefficients of 0.06 below 90 ºC and 0.12 above 110 ºC are used.

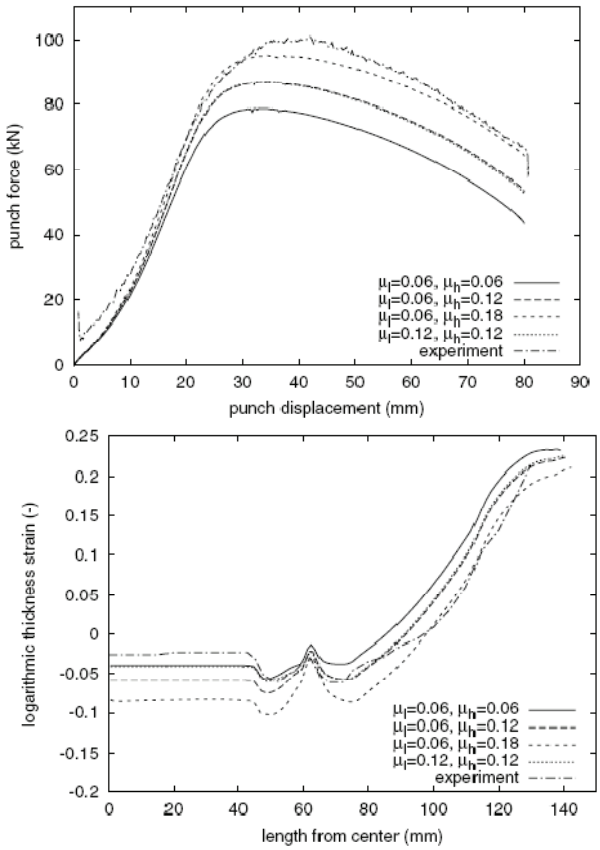

Fig. 7. Influence of friction on calculated force and thickness.

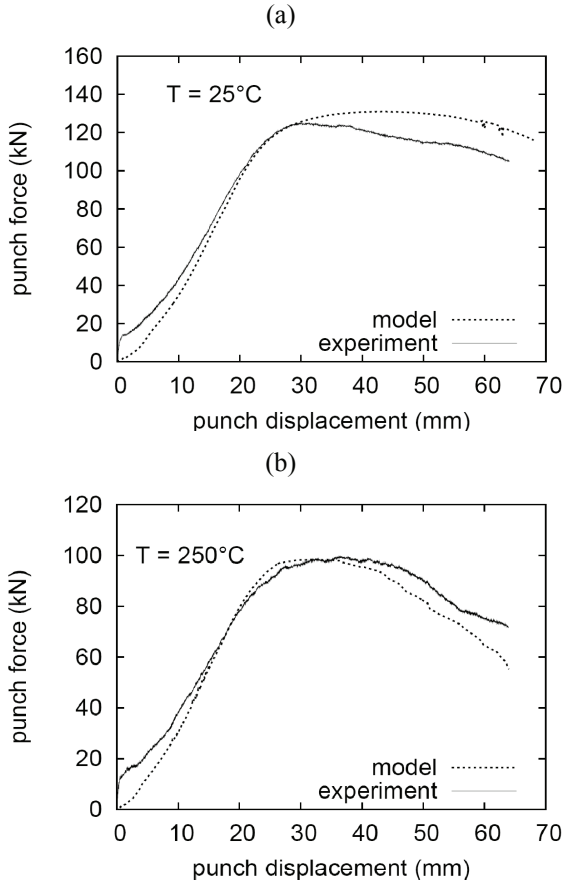

Fig. 8. Punch force-displacement curves from the Nes model compared with experiments.

4.2. Results

In figures 8 and 9, the force–displacement diagrams of the punch and the thickness distributions of the cup at a depth of 64 mm are plotted for the experiments and the simulations. Comparing the different punch force–displacement curves, it can be seen that the general trends with changing temperature are predicted well. However, at 25 ºC the punch force is overestimated after highest point of the experimental curve as shown in figure 8(a). At 250 ºC the punch force is underestimated after the highest point of experimental curve as shown in figure 8(b). The thickness distribution vs. distance from the centre of the cup is shown in figure 9. At room temperature a good agreement can be observed for the wall thickness but the thickness is underestimated in the bottom of the cup, see figure 9(a). At high temperatures the bottom thickness increases, while the wall thickness reduces compared to room temperature. It is observed that this trend is also represented by the model, but the effect is overestimated as shown in figure 9(b).

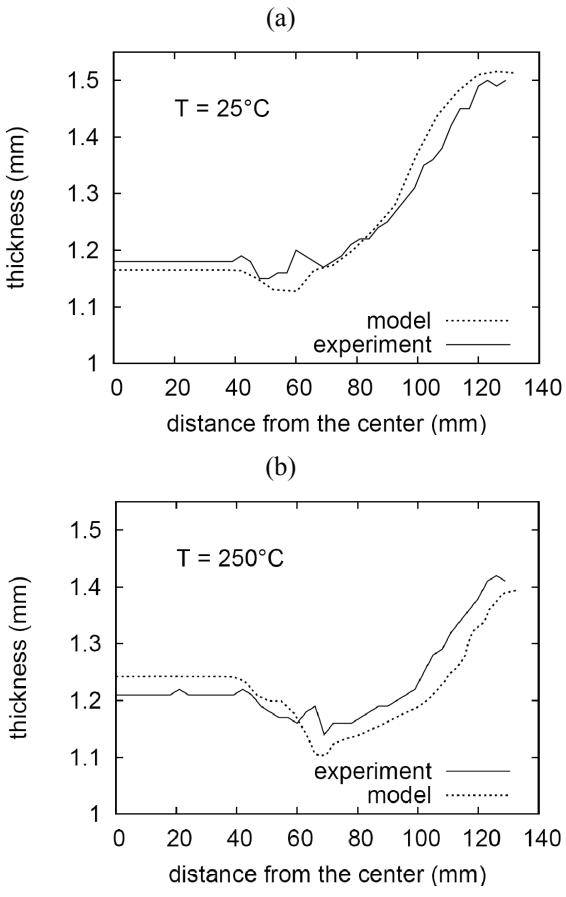

Fig. 9. Thickness distribution curves from the Nes model compared with experiments.

ACKNOWLEDGEMENTS

This research was carried out under the project number MC1.02106 in the framework of the Research Program of the Materials innovation institute M2i (www.m2i.nl), the former Netherlands Institute for Metals Research. The financial support from Materials Innovation Institute, M2i, Netherlands, is highly acknowledged. The authors are indebted to P.J. Bolt and R. Werkhoven of TNO Science and Industry for performing the warm deep drawing experiments.

REFERENCES

1. Abedrabbo, N., Pourboghrat, F., Carsley, J., Forming of AA 5182-O and AA 5754-O at elevated temperatures using coupled thermo-mechanical finite element models, Int. J. of Plast., 23, 2007, 841–875.
2. Ayres, R., Alloying aluminum with magnesium for ductility at warm temperatures (25 to 250°C), Metall. Trans. A, 10, 1979, 849–854.
3. Bolt, P.J., Lamboo, N.A.P.M., Rozier, P.J.C.M., Feasibility of warm Drawing of Aluminum Products, J. Mat. Proc. Tech., 115, 2001, 118–221.
4. Li, D., Ghosh, A.K., Biaxial warm forming behavior of aluminum sheet, J. Mat. Proc. Tech., 145, 2004, 281–293.
5. Van den Boogaard, A.H., Huétink, J., Simulation of aluminum sheet forming at elevated temperatures, Comp. Methods. in App. Mech. and Engg., 195, 2006, 6691–6709.
6. Lebensohn, R.A., Tomé, C.N. A self-consistent anisotropic approach for the simulation of plastic deformation and texture development of polycrystals: Application to zirconium alloys, Acta Metall. Et Mater., 41(9), 1993, 2611–2624.
7. Vegter, H., Van den Boogaard, A.H., A plane stress yield function for anisotropic sheet material by interpolation of biaxial stress states, Int. J. Plast., 2006, 22, 557–580.
8. Nes, E., Modeling of work hardening and stress saturation in FCC metals, Prog. in Mat. Sci., 145, 1998, 129-193.
9. Holmedal, B., Marthinsen, K., Nes, E., A unified microstructural metal plasticity model applied in testing, processing, and forming of aluminum alloys, Z. Metallkd., 96, 2005, 532–545.
10. Nes, E., Marthinsen, K., Modeling the evolution in microstructure and properties during plastic deformation of FCC-metals and alloys—an approach towards a unified model, Mat. Sci. and Engg. A, 322, 2002, 176–193.

TERMOMECHANICZNA OBRÓBKA PLASTYCZNA BLACH Al-Mg-Si

Streszczenie

Temperatura oraz rozkład prędkości odkształcenia podczas formowania aluminium na ciepło charakteryzują się duża niejednorodnością. Wykorzystywane do analizy modele naprężenia uplastyczniającego powinny uwzględniać wpływ tych niejednorodności. Opracowany w niniejszej pracy fizyczny model Nes wykorzystano do symulacji tłoczenia aluminium AA6061-T4 w warunkach odkształcenia na ciepło. W trakcie analizy zaobserwowano znaczące różnice w kształcie wypływki uzyskanej podczas odkształcenia w temperaturze pokojowej oraz 250 ºC. Analiza z wykorzystaniem modelu plastyczności kryształów wykazała aktywności dodatkowych systemów poślizgu w podwyższonych temperaturach. W pracy przedstawiono wyniki analizy numerycznej dla procesów rozciągania oraz tłoczenia.

Submitted: October 1, 2008
Submitted in a revised form: November 3, 2008
Accepted: November 3, 2008